17th World Conference on Earthquake Engineering, 17WCEE

Sendai, Japan - September 13th to 18th 2020

VERIFICATION OF NUMERICAL MODELS FOR SEISMIC FLUID-STRUCTURE INTERACTION OF ADVANCED REACTOR INTERNALS

C.-C. Yu[(1)], F.U.H. Mir[(2)], A.S. Whittaker[(3)]

[(1)] *Doctoral Student, Department of Civil, Structural, and Environmental Engineering, University at Buffalo, cyu23@buffalo.edu*

[(2)] *Doctoral Student, Department of Civil, Structural, and Environmental Engineering, University at Buffalo, faizanul@buffalo.edu*

[(3)] *SUNY Distinguished Professor, Department of Civil, Structural, and Environmental Engineering, University at Buffalo, awhittak@buffalo.edu*

Abstract

Earthquake shaking of a fluid-filled advanced reactor induces fluid-structure interaction (FSI) between the reactor vessel, the submerged internal components, and the contained fluid. Numerical models for FSI analysis will be required for seismic design and qualification of the advanced reactors in part because of the limitation of analytical solutions and physical testing. Analytical solutions cannot accommodate realistic geometry and boundary conditions of the vessel and its internal components, three-directional seismic input, and nonlinear responses of the fluid. The reactor vessels are too large to qualify on available earthquake simulators and pressure loading time series on internal components, immersed in the fluid, are too complex to reproduce with physical testing equipment such as actuators.

Numerical models for FSI analysis need to be first verified and validated before being used for seismic design and qualification of a fluid-filled advanced reactor. A numerical model can be verified by comparing analysis results with those calculated using analytical solutions and validated using data from physical testing. This paper describes 1) prior analytical work on lateral frequencies of submerged internal components, 2) numerical models of an internal component submerged in a fluid confined by the wall of a tank, analyzed using the Incompressible Computational Fluid Dynamics solver in LS-DYNA, and 3) verification of the numerical models by comparing the numerical and analytical results. Validation of the verified models will be performed using data from earthquake simulator tests of a 1/10th-scale, base-supported, cylindrical tank with internal components.

Keywords: seismic fluid-structure interaction; verification of numerical models; advanced reactors; submerged internal components

1. Introduction

Earthquake shaking of a fluid-filled advanced reactor, as presented in Fig. 1 [1], induces fluid-structure interaction (FSI) between the reactor vessel, the contained fluid, and the internal components. Seismic design and qualification of advanced reactors will require verified and validated numerical models for FSI analysis. Realistic geometries and boundary conditions for the vessel and the internal components, three-directional seismic input, and nonlinear responses of the fluid cannot be addressed using analytical solutions. Physical experiments are not practical for testing and qualifying reactors. The reactor vessels are too large to qualify on available earthquake simulators, and pressure loading time series on internal components, immersed in the fluid, are too complex to reproduce with testing equipment such as actuators.

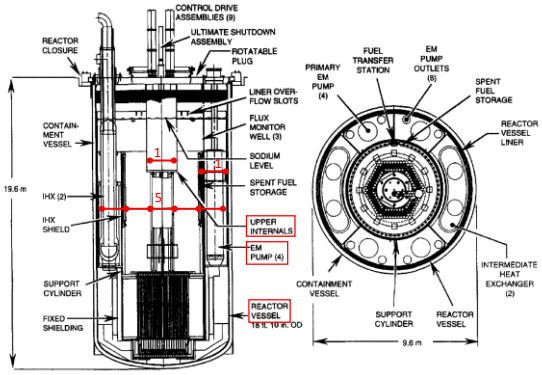

Fig. 1 – Prototype advanced reactor, including a reactor vessel, internal components, and a contained fluid [1]; radius ratios of internal components and the vessel indicated using red lines

Numerical models can be verified by comparing results with those calculated using analytical solutions. A verified numerical model can be validated using data from physical testing. Yu [2] is developing verified and validated models for seismic FSI analysis of advanced reactors, which do not exist at the time of this writing. The numerical models presented in [2] are analyzed using the Arbitrary Lagrangian and Eulerian (ALE) and the Incompressible Computational Fluid Dynamics (ICFD) solvers in LS-DYNA [3], both of which are capable of calculating nonlinear FSI responses. The verification studies for reactor vessels and internal components are conducted separately [2] since there is no comprehensive analytical solutions capable of addressing their interaction with the presence of contained fluid. Yu et al. [4, 5] present the verification study for ALE models of a reactor vessel (i.e., vertical cylindrical tank), for which the numerical results were compared with those calculated using prior and newly-developed analytical solutions [6-9]. The verified ALE models were validated using data from earthquake simulator tests [10], involving a 1/10th-scale, base-supported, cylindrical, steel tank filled with water, as shown in Fig. 2a. The geometry of this 1/10-scale test tank is loosely based on those of prototype liquid metal reactor vessels.

(a) base-supported steel tank filled with water: radius of 0.79 m, height of 2 m, wall thickness of 8 mm

(b) central internal component: round HSS 12.75× 0.25 steel pipe [11], radius of 0.162 m, height of 1.5 m, wall thickness of 6.35 mm

Fig. 2 – Earthquake simulator tests, 1/10th-scale model

This paper verifies ICFD models for an internal component submerged in a fluid confined by the wall of a tank. The dimensions used in the models are based on those used for earthquake simulator tests [12]: the 1/10th-scale model tank of Fig. 2a and the central internal component supported at the head of the tank, shown in Fig. 2b. The radius of the internal component is about 1/5th of that of the test tank. Per Fig. 1, internal components are generally vertical, cylindrical, pipe-type structures, and the red lines in the figure indicate that the ratio of the radii of the internal components to the vessel is about 1/5. The ICFD models are verified using the analytical solutions of Chen and Rosenberg [13] for lateral frequencies of the submerged internal component. To adopt the assumptions made in [13] and enable verification, the heights and boundary conditions of the tank and the internal component are assumed to be identical, and the internal component is assumed to be filled with fluid. (In the experiments, the heights and boundary conditions are different, and the internal component is not filled with fluid; see [12] for more information.) Validation of the verified ICFD models will be performed using data generated by the earthquake simulator tests for specimens including those shown in Fig. 2.

2. Analytical study

Chen and Rosenberg [13] derived analytical solutions for frequencies of two concentric pipes filled with fluid, as shown in Fig. 3a. The fluid fully filled both the inside of the inner pipe and the annulus between the pipes. For application to design and analysis of a nuclear reactor, the inner pipe was considered to be an internal component, and the outer pipe to be the wall of the reactor vessel. The lengths and boundary conditions of the two pipes were assumed to be identical. The pipes were assumed to be either elastic or rigid with a constant thickness; the fluid was assumed to be ideal, namely, inviscid and incompressible. Although 1) a reactor vessel and its internal components are generally not concentric, 2) their boundary conditions and lengths are not identical, and 3) the fluid does not fully fill the vessel, [13] provided the most relevant information for design and analysis of internal components in an advanced reactor[1], to the knowledge of the authors of this paper.

When the pipes displace (e.g., due to seismic motions), the fluid adjacent to them generates hydrodynamic pressures on their surfaces. Fig. 3b presents the hydrodynamic pressures on the inner and outer pipes on a $x-y$ plane. The mass of the fluid contributing to the hydrodynamic pressures was assumed to be attached to and move with the pipes, which reduced their frequencies (i.e., the so-called *added mass effect*). The hydrostatic pressure on the pipes and free surface were not considered since gravity was not included in the analysis. Note that in Fig. 3b, "Pipe 1" refers to the inner pipe, "Pipe 2" refers to the outer pipe, "Fluid 1" refers to the fluid inside the inner pipe, and "Fluid 2" refers to the fluid filling the annulus between the two pipes. These numberings are consistent with the subscripts of the variables using in the analytical solutions presented here and in [13]. For the inner pipe (i.e., Pipe 1), the radius, height, and wall thickness are R_1, H_1, and h_1, respectively, and the density, elastic modulus, Poisson's ratio are ρ_{s1}, E_1, and υ_1, respectively. For the outer pipes (i.e., Pipe 2), the variables are defined by substituting "2" for the subscript "1" of the corresponding variables for the inner pipe. Since the heights of the two pipes are identical, a variable H is used for both pipes (i.e., $H = H_1 = H_2$). The densities of Fluids 1 and 2 are ρ_1 and ρ_2, respectively.

Chen and Rosenberg used the equations of equilibrium for cylindrical shells provided by Flugge [15] to relate the displacements of the pipes to their inertial forces and hydrodynamic forces (i.e., resultant forces of hydrodynamic pressures). Three degrees of freedom were considered for each pipe (i.e., six degrees of freedom for the two pipes), associated with the respective r, θ, and z axes presented in Fig. 3a. Based on the equations of equilibrium (i.e., equation of motion) presented in [13], the mass and stiffness matrices of the two pipes filled with fluid, $[M]$ and $[K]$, are extracted here in. The mass matrix, $[M]$, includes the masses of the pipes and the added masses attached to the pipes generated by the hydrodynamic pressures shown in Fig. 3b. The stiffness matrix, $[K]$, is formed by the two pipes only since fluid has no stiffness. The

[1] Section 3.6 of ASCE/SEI 4-16 [14] uses the analytical solutions of Chen and Rosenberg [13], in part, to provide guidance for the analysis and design of submerged nuclear components.

entries for $[M]$ and $[K]$ are presented in the appendix, and they are functions of the mechanical properties and dimensions of the two pipes and the fluid and an assumed wavelength[2] for the modal shapes of the two pipes. The derivation of the entries is not presented in this paper but can be found in Yu (in progress) with corrections to the calculation errors made in [13].

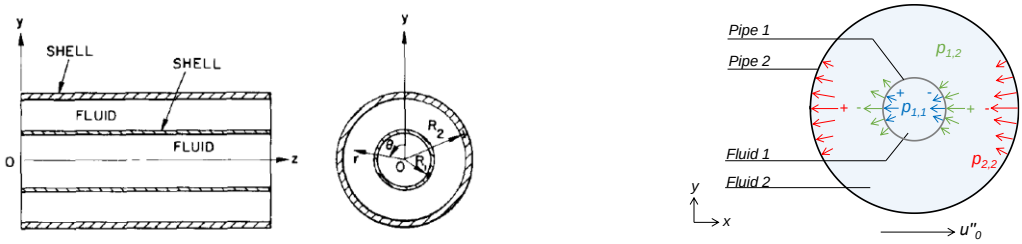

(a) Chen and Rosenberg [13], $y-z$ and $x-y$ views

(b) hydrodynamic pressures on the two pipes, accelerating in the x direction, $x-y$ view

Fig. 3 – Two concentric cylindrical pipes with fluid fully filling the inside of the inner pipe and the annulus between the two pipes

Given $[M]$ and $[K]$, the angular frequencies, ω, associated with the assumed wavelength of the two fluid-filled pipes (e.g., $l = 3.351\,H$ for the modal shape presented in figure (a) in footnote 2) are calculated by:

$$eig\left(\left[M\right]^{-1}\left[K\right]\right) \rightarrow (\omega^2, \phi) \tag{1}$$

where $eig(\cdot)$ is the operator for calculating the eigenvalues and eigenvectors of a matrix. The dimensions of $[M]^{-1}[K]$ are 6×6 and so Eq. (1) leads to six eigenvalues and six eigenvectors. The square roots of the eigenvalues calculated using Eq. (1) are the angular frequencies ω of the two fluid-filled pipes. The corresponding frequencies of the pipes are $f = \omega / 2\pi$. The modal shapes, ϕ, account for the interaction of the responses of the pipes and the fluids. The modal shapes, ϕ, associated with the lowest two values of ω involve coupled lateral movements of the two pipes associated with the assumed wavelength used in the calculation. These two modes, with the two lowest values of ω, are termed "coupled modes" hereafter. The other four frequencies and modal shapes are associated with axial and torsional motions of each pipe, which are not the focus here and not discussed further. The shape of the first coupled mode involves *out-of-phase* motions of the two pipes, and that of the second coupled mode involves *in-phase* motions. Fig. 4 illustrates the motion of the two pipes in the two coupled modes in a $x-y$ view. In the out-of-phase mode, the outer and inner pipes displace in opposite directions. In the in-phase mode, the two pipes displace in the same direction.

[2] The wavelength l of a pipe is not the length (e.g., height) of the pipe, which was misused in some prior studies. The wavelength represents the shape in a given mode of an elastic beam with a uniform cross section. Wavelengths in different lateral modes were theoretically derived in [16] for a beam with the two ends 1) pinned-pinned (i.e., simply supported), 2) fixed-fixed, 3) fixed-free (i.e., cantilever beam), and 4) fixed-pinned. The wavelengths of the first lateral modal shapes (blue) of a cantilever and a simply-supported beam (black) are illustrated below:

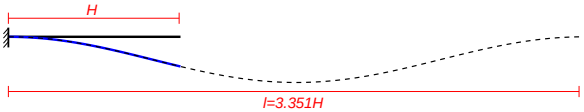

(a) cantilever beam, $l = 3.351\,H$

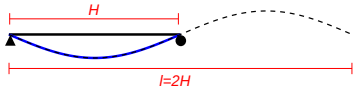

(b) simple-supported beam, $l = 2\,H$

Fig. 4 – Modal shapes of coupled lateral motions, out-of-phase and in-phase, two fluid-filled concentric pipes, $x-y$ view

If the outer pipe is rigid relative to the inner pipe[3], the frequencies of the inner pipe can be calculated using the 3×3 submatrices of $[M]$ and $[K]$ associated with its three degrees of freedom (i.e., entries associated with the degrees of freedom of the outer pipe are omitted). The 3×3 submatrices are termed $[M_1]$ and $[K_1]$ here. See the appendix for the entries of $[M_1]$ and $[K_1]$. Three angular frequencies ω are calculated through Eq. (1) using $[M_1]$ and $[K_1]$. The lowest value of ω is associated with a lateral mode of the inner pipe and the other two are associated with an axial and a torsional mode. Although the degrees of freedom of the outer pipe are not involved in the calculation, its radius defines the volume of the fluid and the added mass, which affects the frequencies of the inner pipe. Consequently, the radius of the outer pipe is involved in $[M_1]$ (see α_2 in entry m_{11} of $[M_1]$).

2.1 Analytical calculation and results

Lateral frequencies and modal shapes of two fluid-filled concentric pipes are calculated using the analytical solutions of [13]. The dimensions and mechanical properties of the steel tank (i.e., outer pipe), central internal component (i.e., inner pipe), and contained fluid of Fig. 2 are used in the calculation. However, to adopt the assumptions made in [13], the two pipes are assumed to be both top-supported (i.e., cantilever), which is similar to the boundary conditions of some advanced reactors (see Fig. 1), and their heights are identical (i.e., $H = H_1 = H_2$). The height of a half to full test tank is used for the calculation: 1 m $\le H \le$ 2 m. The dimensions and the mechanical properties used for the calculation are presented in Table 1. To calculate lateral frequencies associated with the first wavelength of cantilevers, $l = 3.351\,H$ is used in the calculation (see footnote 2).

Table 1 – Dimensions and mechanical properties used for the analytical solutions and the numerical models presented in Section 3, materials for Pipes 1 and 2 are both carbon steel, Fluids 1 and 2 are both water

R_1 (m)	R_2 (m)	h_1 (mm)	h_2 (mm)	$H_1 = H_2 = H$ (m)
0.162	0.79	6.35	7.92	1 to 2[1]
E_1, E_2 (N/m^2)	ρ_{s1}, ρ_{s2} (kg/m^3)	υ_1, υ_2	ρ_1, ρ_2 (kg/m^3)	μ_1, μ_2 [2]
2×10^{11}	7850	0.27	1000	0

1. $H = 2$ m is used for the numerical models
2. Fluid is assumed to be inviscid for the analytical solutions

Fig. 5a presents the lateral frequencies for 1) the two coupled modes of the two pipes (out-of-phase and in-phase) and 2) the uncoupled mode of the inner pipe considering the outer pipe to be rigid. For the coupled modes, for a given value of H, the frequency in the out-of-phase mode (red solid line) is appreciably lower than that in the in-phase mode (blue solid line). The frequency of the uncoupled mode of the inner pipe (black dotted line) is almost identical to that of the out-of-phase mode, for the dimensions and mechanical properties used here (see Table 1). Fig. 5b presents the the amplitudes of the lateral modal shapes associated with the frequencies shown in Fig. 5a. The amplitudes are normalized by that for the inner pipe in the uncoupled mode. At a given value of H, the amplitude of the inner pipe in the out-of-phase mode (red solid line) is identical to that of the uncoupled mode (black dotted line), and the amplitude of the outer pipe (red dashed line) is almost zero. This outcome indicates that for the dimensions and mechanical properties

[3] This assumption is made in ASCE 4-16 for FSI analysis of internal components (i.e., inner pipe) submerged in a fluid contained in a tank or reactor vessel (i.e., rigid outer pipe). The tank (reactor vessel) is assumed to be rigid relative to their internal components.

considered here, in the out-of-phase mode, the movement of the inner pipe is much greater than that of the outer pipe, which can be assumed to be rigid. In the in-phase mode, the amplitudes of the two pipes (blue solid and dashed lines) are not significantly different, and both smaller than the amplitudes of the inner pipe in the uncoupled and out-of-phase modes (red solid and black dotted lines).

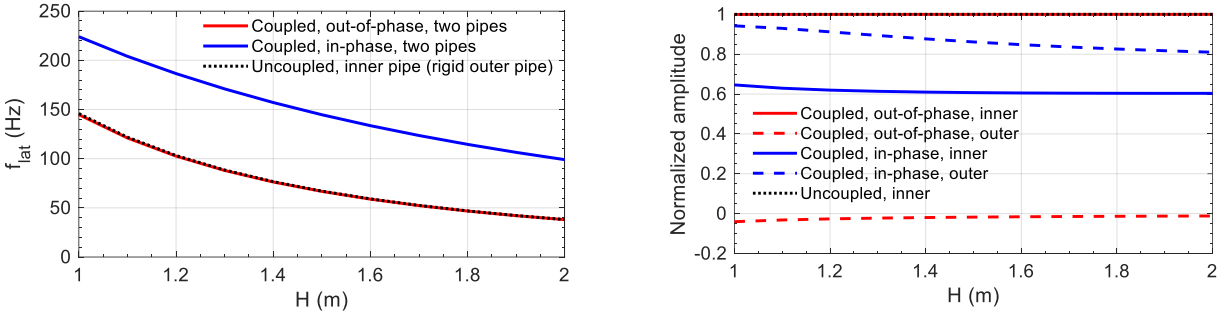

(a) lateral frequencies (b) normalized amplitudes of lateral modal shapes

Fig. 5 – Modal properties of two fluid-filled concentric pipes calculated using the variables presented in Table 1, the first wavelength $l = 3.351\,H$

3. Numerical analysis

3.1 Numerical models

Numerical models of two fluid-filled cylindrical pipes are analyzed. The pipes are concentric and supported at the top. The ICFD solver in LS-DYNA is used to performed FSI analysis to determine the lateral frequencies of the inner pipe. The variables presented in Table 1 and used for the analytical calculations in Section 2.1, are used for the models to enable comparisons of analytical and numerical results.

Fig. 6 presents the numerical models and the global coordinate system (x, y, z). Fig. 6a shows the finite elements for the inner pipe (green) and the outer pipe (blue). The model of the contained fluid is defined by its boundaries, which are surfaces enclosing the fluid. Fig. 6b presents a half model to show these fluid surfaces: 1) adjacent to the outer pipe (yellow), 2) adjacent to the inner pipe (light blue), 3) horizontally at the top of the two pipes (pink), and 4) horizontally at the base of the two pipes (dark blue). The pipes are constructed using Lagrangian four-node shell elements and the fluid surfaces are constructed using Lagrangian three-node shell (i.e., triangular) elements. The pipes and the fluid surfaces do not share nodes at their interfaces. The *ICFD_BOUNDARY_FREESLIP card in the LS-DYNA deck is assigned to all fluid surfaces to model frictionless boundaries. The *MESH_EMBEDSHELL card is assigned to the fluid surface adjacent to the inner pipe to model the fluid domain seperated by by the submerged shell elements of the inner pipe. The fluid domain is automatically meshed using Lagrangian, four-node, solid (i.e., tetrahedral) elements by the ICFD solver at the first step of the analysis (i.e., $t = 0$): see Fig. 6c.

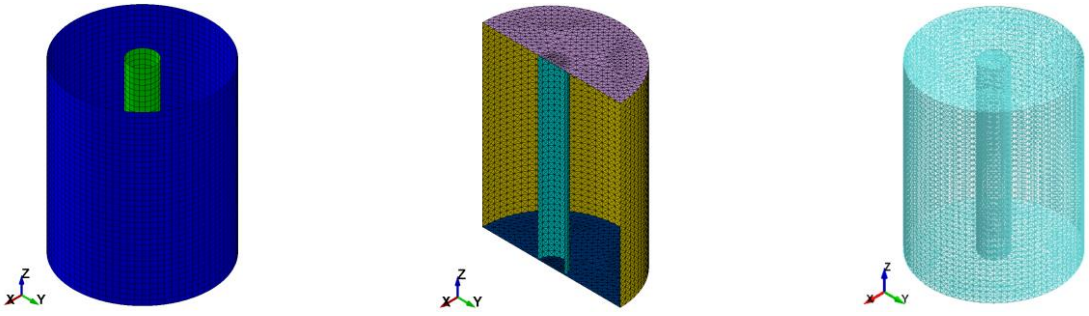

(a) pipes (b) fluid surfaces (c) fluid, $t = 0$

Fig. 6 – ICFD model, two concentric pipes, fluid filling between the pipes and in the inner pipe

Lateral frequencies are calculated for 1) the two modes involving coupled movements of the two pipes (i.e., out-of-phase and in-phase modes), and 2) the uncoupled mode of the inner pipe. Two ICFD models of Fig. 6 are used for the analysis. To calculate the two coupled frequencies, the elements of both pipes in the first model are assigned to be elastic. To calculate the uncoupled frequency, in the second model, the elements of the inner pipe are assigned to be elastic and those of the outer pipe are assigned to be rigid. The masses of the inner and outer pipes are 49 and 629 kg, respectively, and that of the fluid is 3921 kg in each model. No damping is assigned to the pipes. No gravitational acceleration is assigned to the models since gravity was not considered in the analytical solutions.

The ICFD solver cannot perform eigenvalue analysis, and so lateral frequencies are identified from the response histories of the submerged component (i.e., inner pipe) undergoing free vibration. To achieve free vibration response, the displacement time series shown in Fig. 7a is applied at the free (i.e., bottom) end of the inner pipe in the x direction, and the pipe is then released to vibrate. The peak displacement is 15 mm (i.e., at 0.03 sec in Fig. 7a), which is less than 1% of the height of the inner pipe ($0.01\,H = 20$ mm). This displacement generates the lateral modal shape of the first wavelength (i.e., $l = 3.351\,H$), and the associated frequencies (i.e., two coupled and one uncoupled) are the focus of the analysis and verification. The circumferential, axial, and torsional modes are not considered. A rigid diaphragm is assigned to the nodes at the free end of the inner pipe through *CONSTRAINT_NODAL_RIGID_BODY card, as shown in Fig. 7b. The displacement time series is applied at the center of the diaphragm. The rigid diaphragm makes the assigned set of nodes translate and rotate as a rigid body, and prevents circumferential deformation due to the applied displacement. Response-history analysis of each model is performed for about 2 seconds after the pipe is released (i.e., at 0.03 sec in Fig. 7a) to vibrate freely. The displacement time series of the free vibration at the center of the rigid diaphragm is transformed to the frequency domain using the Fast Fourier Transform (FFT), and the frequency in each lateral mode of the inner pipe in each model is identified from the Fourier amplitude spectrum.

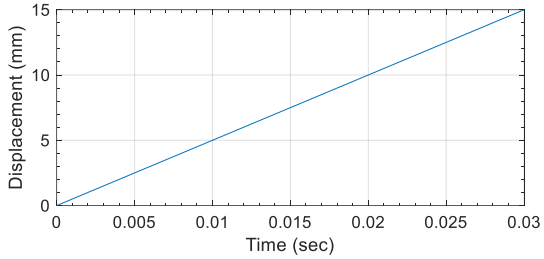

(a) displacement time series

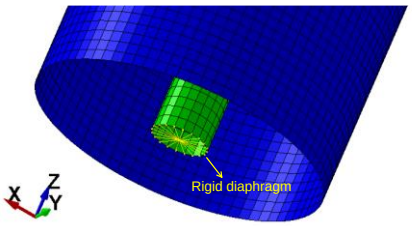

(b) rigid diaphragm (yellow lines)

Fig. 7 – Input motion applied at the center of the rigid diaphragm at the free end of the inner pipe

3.2. Results and verification

Fig. 8 present Fourier amplitude spectra for the displacement time series at the center of the rigid diaphragm of the inner pipe for the two models. The displacement time series is a first-mode free vibration response. Each Fourier amplitude spectrum shown in Fig. 8 is normalized by its maximum ordinate. The peak in each Fourier amplitude spectrum is associated with the lateral frequency of the inner pipe. The frequency in the first coupled mode is identified using the spectrum in blue (i.e., 37 Hz), but that in the second coupled mode cannot be identified because the displacement amplitude in the mode is too small. The frequency in the uncoupled mode (red spectrum) is 37 Hz.

As noted in Section 2.1 for Fig. 5a, the frequency in the first coupled mode (i.e., the out-of-phase mode) is identical to that in the uncoupled mode of the inner pipe for the dimensions and the mechanical properties of the pipes and fluid considered here (see Table 1). The outer pipe can be considered to be rigid. The second coupled mode (i.e., the in-phase mode) cannot be identified from the blue spectrum because the lateral movement of the inner pipe in this mode is insignificant, with respect to that in the first coupled mode.

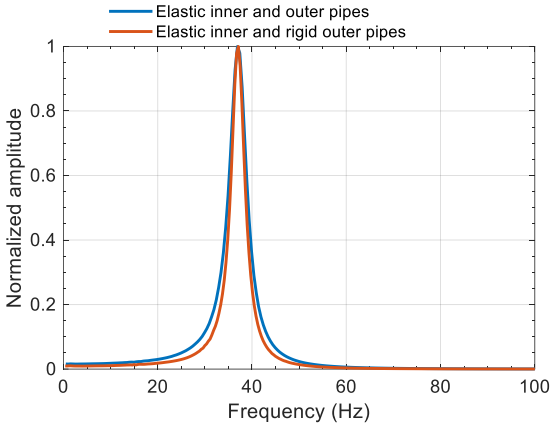

Fig. 8 – Normalized Fourier amplitude spectra for the displacement time series at the center of the rigid diaphragm of the inner pipe in the ICFD models

Table 2 compares the results of analysis of the ICFD models and the analytical solutions [13]. The frequencies calculated using the analytical solutions are listed in the second column, which are extracted from the results presented in Fig. 5a at $H = 2$ m. The corresponding frequencies identified from the Fourier amplitude spectra in Fig. 8 for the ICFD models are listed in the third column. The frequency in the coupled in-phase mode cannot be identified through the blue spectrum in Fig. 8 and so is not listed in the table. The differences between the ICFD and the analytical results are very small, and listed in the fourth column.

Table 2 – Coupled and uncoupled lateral frequencies of the inner pipe, calculated using the analytical solutions [13] and the ICFD models

Mode	Frequency (Hz)		Difference[1] (%)
	Analytical solutions	ICFD model	
First coupled, out-of-phase	38	37	-2
Second coupled, in-phase	99	--	--
Uncoupled	38	37	-2

1. Percentage differences of the numerical results with respect to those calculated using the analytical solutions

4. Summary and conclusions

The seismic design and qualification of advanced nuclear reactors and their internal components will rely on verified and validated numerical models that can accommodate three-directional seismic inputs. This paper verifies numerical models performed using the ICFD solver in LS-DYNA for an internal component submerged in a fluid confined by the wall of a cylindrical tank. The dimensions and geometries used in the numerical models are based on the corresponding specimens shown in Fig. 2 for earthquake simulator tests: a 1/10th-scale base-supported cylindrical tank and a pipe-type central internal component supported at the top by the head of the tank. To enable comparisons between numerical and analytical results, identical heights and boundary conditions (i.e., top-supported) are used for the tank and the internal component in the models, consistent with the assumptions made for the analytical solutions used in this paper.

The analytical solutions developed by Chen and Rosenberg [13] for frequencies of two concentric cylindrical pipes are used here for verification. Fluid filled the inside of the inner pipe and the annulus between the two pipes, as shown in Fig. 3. The inner pipe was assumed to be an internal component and the outer pipe to be the wall of a tank (reactor vessel). The lengths and boundary conditions of the two pipes were assumed to be identical. The analytical solutions [13] addressed the lateral, torsional, and axial frequencies of the two fluid-filled pipes, and lateral frequencies are the focus of the verification. If both pipes are flexible (elastic), their lateral motions involve two coupled modes: out-of-phase and in-phase as shown in Fig. 4. If the inner pipe is flexible and the outer pipe is rigid, the lateral motion of the inner pipe involves one uncoupled mode. For the dimensions, mechanical properties, and boundary condition (i.e., top-supported)

considered in the calculation, the frequency in the out-of-phase mode is appreciably lower than that in the in-phase mode. The frequency in the uncoupled mode of the inner pipe is almost identical to that in the out-of-phase mode.

The seismic FSI analysis of a submerged internal component is performed for two numerical models and the lateral frequencies are calculated. In the first model, the elements of both pipes are assigned to be elastic to calculate the two coupled frequencies. In the second model, the elements of the inner pipe are assigned to be elastic and those of the outer pipe are assigned to be rigid to calculate the uncoupled frequency. The ICFD solver cannot perform eigenvalue analysis and so frequencies are identified from the Fourier amplitude spectra for free vibration response histories of the internal component. The differences of the first coupled and uncoupled frequencies calculated using the numerical models and the analytical solutions are about 2%. The tiny differences between the numerical and analytical results enable the authors to conclude that the ICFD models are verified, for submerged components of geometries and dimensions similar to those used here. The verified ICFD models will be validated using dataset generated by the earthquake simulator tests presented in [12]. Other verification studies can be found in [2], including numerical models for rigid and flexible tanks and other internal components analyzed using both the ALE and ICFD solvers in LS-DYNA.

5. Acknowledgements

The information, data, or work presented herein was funded in part by the Advanced Research Projects Agency-Energy (ARPA-E), U.S. Department of Energy, under Award Number DE-AR0000978, and in part by TerraPower and the U.S. Department of Energy under CRADA 14CR04. The views and opinions of the authors expressed herein do not necessarily state or reflect those of the United States Government or any agency thereof, or TerraPower.

6. Appendix

This appendix presents the equation of motion and the associated mass and stiffness matrices of two fluid-filled concentric pipes shown in Fig. 3. Calculation errors involved in the derivation of [13] are corrected, and the matrices presented here are extracted from the corrected equation of motion. The derivation with corrections are not presented but can be found in [2].

The equation of motion of the two fluid-filled concentric pipes shown in Fig. 3 is:

$$[M]\{\ddot{q}\}+[K]\{q\}=0 \tag{2}$$

where $[M]$ and $[K]$ are the mass and stiffness matrices, $\{q\}$ is the displacement vector of the two pipes associated with the considered degrees of freedom, and $\{\ddot{q}\}$ is the second derivative of $\{q\}$ with respect to time. The vector $\{q\}$ is composed of the radial, angular, and axial displacements (i.e., u_s, v_s, and w_s) of the inner and outer pipes in the r, θ, and z axes, respectively, namely, $\{q\}=\{u_{s1},v_{s1},w_{s1},u_{s2},v_{s2},w_{s2}\}^T$. The dimensions of $[M]$ and $[K]$ are 6×6 and can be used to calculate frequencies of the two fluid-filled pipes per Eq. (1). The entries in the two matrices are functions of the dimensions and mechanical properties of the two pipes and the fluid. Variables for the entries include the radii, R_1 and R_2, thicknesses, h_1 and h_2, height, H ($H=H_1=H_2$), densities, ρ_{s1} and ρ_{s2}, elastic moduli, E_1 and E_2, and Poisson's ratios, υ_1 and υ_2, of the two pipes (i.e., Pipes 1 and 2 shown in Fig. 3b), and the densities, ρ_1 and ρ_2, of the two fluids (i.e., Fluids 1 and 2 shown in Fig. 3b).

The entries of $[M]$ are:

$$[M]_{6\times6}=\begin{bmatrix} m_{11} & 0 & 0 & m_{14} & 0 & 0 \\ 0 & m_{22} & 0 & 0 & 0 & 0 \\ 0 & 0 & m_{33} & 0 & 0 & 0 \\ m_{41} & 0 & 0 & m_{44} & 0 & 0 \\ 0 & 0 & 0 & 0 & m_{55} & 0 \\ 0 & 0 & 0 & 0 & 0 & m_{66} \end{bmatrix} \tag{3}$$

$$m_{11}=\frac{R_1^2\rho_{s1}(1-\upsilon_1^2)}{E_1}\cdot\left(1+\frac{\rho_1}{h_1\rho_{s1}}\frac{I_1(\alpha_1)}{I_1'(\alpha_1)}-\frac{\rho_2}{h_1\rho_{s1}}\frac{I_1(\alpha_1)K_1'(\alpha_2)-K_1(\alpha_1)I_1'(\alpha_2)}{I_1'(\alpha_1)K_1'(\alpha_2)-K_1'(\alpha_1)I_1'(\alpha_2)}\right) \tag{4}$$

$$m_{22}=\frac{R_1^2\rho_{s1}(1-\upsilon_1^2)}{E_1} \tag{5}$$

$$m_{33}=-\frac{R_1^2\rho_{s1}(1-\upsilon_1^2)}{E_1} \tag{6}$$

$$m_{44}=\frac{R_2^2\rho_{s2}(1-\upsilon_2^2)}{E_2}\cdot\left(1+\frac{\rho_2}{h_2\rho_{s2}}\frac{K_1(\alpha_2)I_1'(\alpha_1)-I_1(\alpha_2)K_1'(\alpha_1)}{I_1'(\alpha_1)K_1'(\alpha_2)-K_1'(\alpha_1)I_1'(\alpha_2)}\right) \tag{7}$$

where $\alpha_1=2\pi R_1/l$ and $\alpha_2=2\pi R_2/l$; l is an assumed wavelength for the modal shapes of the pipes; I_1 and K_1 are modified Bessel's functions of the first and second kind, respectively; and I_1' and K_1' are the first derivatives of $I_1(2\pi r/l)$ and $K_1(2\pi r/l)$ with respect to r, respectively. Entries m_{55} and m_{66} are counterparts of m_{22} and m_{33}, respectively. Entries m_{55} and m_{66} are calculated by replacing the dimensions and mechanical properties of Pipe 1 with those of Pipe 2 (i.e., substituting the subscript "1" of each variable with "2").

Entries m_{14} and m_{41} couple the responses of the two pipes due to the presence of Fluid 2 in the annulus between them. Entry m_{14} relates the hydrodynamic pressure on Pipe 1 to the radial displacement of Pipe 2, and m_{41} relates the hydrodynamic pressure on Pipe 2 to the radial displacement of Pipe 1. Entries m_{14} and m_{41} are:

$$m_{14}=-\frac{R_1^2\rho_{s2}(1-\upsilon_1^2)}{E_1}\frac{\rho_2}{h_1\rho_{s1}}\frac{K_1(\alpha_1)I_1'(\alpha_1)-I_1(\alpha_1)K_1'(\alpha_1)}{I_1'(\alpha_1)K_1'(\alpha_2)-K_1'(\alpha_1)I_1'(\alpha_2)} \tag{8}$$

$$m_{41}=\frac{R_2^2\rho_{s2}(1-\upsilon_2^2)}{E_2}\cdot\frac{\rho_2}{h_2\rho_{s2}}\frac{I_1(\alpha_2)K_1'(\alpha_2)-K_1(\alpha_2)I_1'(\alpha_2)}{I_1'(\alpha_1)K_1'(\alpha_2)-K_1'(\alpha_1)I_1'(\alpha_2)} \tag{9}$$

Note that the calculation errors involved in the equation of motion written in [13] affect Eqs. (4), (7), (8), and (9). The corrected equations are presented here.

The entries of $[K]$ are:

$$[K]_{6\times6}=\begin{bmatrix} k_{11} & k_{12} & k_{13} & 0 & 0 & 0 \\ k_{12} & k_{22} & k_{23} & 0 & 0 & 0 \\ k_{13} & k_{23} & k_{33} & 0 & 0 & 0 \\ 0 & 0 & 0 & k_{44} & k_{45} & k_{46} \\ 0 & 0 & 0 & k_{45} & k_{55} & k_{56} \\ 0 & 0 & 0 & k_{46} & k_{56} & k_{66} \end{bmatrix} \tag{10}$$

$$k_{11} = 1 + \frac{h_1^2(\alpha_1^4 + 2\alpha_1^2)}{12R_1^2} \tag{11}$$

$$k_{12} = 1 + \frac{h_1^2}{24R_1^2}(3-\upsilon_1)\alpha_1^2 \tag{12}$$

$$k_{13} = -i \cdot \left(\upsilon_1\alpha_1 + \frac{h_1^2}{12R_1}(\alpha_1^3 - \frac{1-\upsilon_1}{2}\alpha_1) \right) \tag{13}$$

$$k_{22} = 1 + \alpha_1^2(\frac{1-\upsilon_1}{2})(1 + \frac{h_1^2}{4R_1^2}) \tag{14}$$

$$k_{23} = -i \cdot \alpha_1 \frac{1+\upsilon_1}{2} \tag{15}$$

$$k_{33} = -\alpha_1^2 - \frac{1-\upsilon_1}{2}(1 + \frac{h_1^2}{12R_1^2}) \tag{16}$$

Entries k_{44}, k_{45}, k_{46}, k_{55}, k_{56}, and k_{66} are counterparts of k_{11}, k_{12}, k_{13}, k_{22}, k_{23}, and k_{33}, respectively. Entries k_{44}, k_{45}, k_{46}, k_{55}, k_{56}, and k_{66} are calculated by replacing the dimensions and mechanical properties of Pipe 1 with those of Pipe 2 (i.e., substituting the subscript "1" of each variable with "2").

If the outer pipe is assumed to be rigid, the entries associated with the degrees of freedom of the outer pipe are omitted. The submatrices associated with the degrees of freedom of the inner pipe, $[M_1]$ and $[K_1]$, are used in Eq. (1) to calculate frequencies:

$$[M_1]_{3\times3} = \begin{bmatrix} m_{11} & 0 & 0 \\ 0 & m_{22} & 0 \\ 0 & 0 & m_{33} \end{bmatrix} \tag{17}$$

$$[K_1]_{3\times3} = \begin{bmatrix} k_{11} & k_{12} & k_{13} \\ k_{12} & k_{22} & k_{23} \\ k_{13} & k_{23} & k_{33} \end{bmatrix} \tag{18}$$

7. References

[1] Gluekler, E. L. (1997). "U.S. advanced liquid metal reactor (ALMR)." *Progress in Nuclear Energy*, 31(1-2), 43-61.

[2] Yu, C.-C. (in progress). "Verification and validation of numerical models for seismic fluid-structure-interaction analysis of liquid metal reactors." Dissertation, presented to University at Buffalo, in partial fulfillment of the requirements for the degree of Doctor of Philosophy.

[3] Livermore Software Technology Corporation (LSTC) (2019). "LS-DYNA SMP_d_R11_139066." Livermore, CA.

[4] Yu, C.-C., Whittaker, A. S., Coleman, J. L. and Cohen, M. (2018). "Verification of a fluid-structure-interaction model for seismic analysis of Gen IV nuclear power plants." *Proc., 11th National Conference in Earthquake Engineering (11NCEE)*, Los Angeles, CA.

[5] Yu, C.-C., Mir, F. U. H., Cohen, M., Coleman, J. L., Bardet, P. and Whittaker, A. S. (2019). "Verification of numerical models for seismic fluid-structure-interaction analysis of advanced reactors." *Tran., 25th International Conference on Structural Mechanics in Reactor Technology (SMiRT-25)*, Charlotte, NC.

[6] Jacobsen, L. S. (1949). "Impulsive hydrodynamics of fluid inside a cylindrical tank and of fluid surrounding a cylindrical pier." *Bulletin of the Seismological Society of America*, 39(3), 189-204.

[7] Veletsos, A. (1984). "Seismic response and design of liquid storage tanks." *Guidelines for the seismic design of oil and gas pipeline systems*, Committee on Gas and Liquid Fuel Lifelines, American Society of Civil Engineers (ASCE), Reston, VA, 255-370.

[8] Yu, C.-C. and Whittaker, A. S. (submitted in 2019). "Analytical solutions for seismic fluid-structure interaction of head-supported cylindrical tanks." *Submitted to Journal of Engineering Mechanics*.

[9] Yu, C.-C. and Whittaker, A. S. (submitted in 2019). "Review of analytical studies on seismic fluid-structure interaction of base-supported cylindrical tanks." *Submitted to Engineering Structures*.

[10] Mir, F. U. H., Yu, C.-C., Cohen, M., Bardet, P., Coleman, J. and Whittaker, A. (2019). "Dataset generation for validation of fluid-structure interaction models." *Tran., 25th International Conference on Structural Mechanics in Reactor Technology (SMiRT-25)*, Charlotte, NC.

[11] American Institute of Steel Construction (AISC) (2011). *Steel construction manual*, 14th Ed., Chicago, IL.

[12] Mir, F. U. H., Yu, C.-C. and Whittaker, A. S. (2020). "Experiments for validation of FSI models for seismic response of advanced reactor internals." *Tran., 17th World Conference on Earthquake Engineering (17WCEE)*, Sendai, Japan.

[13] Chen, S. and Rosenberg, G. (1975). "Dynamics of a coupled shell-fluid system." *Nuclear Engineering and Design*, 32(3), 302-310.

[14] American Society of Civil Engineers (ASCE) (2017). "Seismic analysis of safety-related nuclear structures and commentary." *ASCE/SEI 4-16*, Reston, VA.

[15] Flugge, W. (1960). *Stresses in shells*, 1st Ed., Springer-Verlag OHG., Berlin/Gottingen/Heidelberg, Germany.

[16] Timoshenko, S. (1937). *Vibration problems in engineering*, 1st Ed., D. Van Nostrand Company, Inc, New York, NY.

